Engineering Structures 97 (2015) 68–79

Contents lists available at ScienceDirect

Engineering Structures

journal homepage: www.elsevier.com/locate/engstruct

Experimental investigation of steel plate shear walls with in-span plastification along horizontal boundary elements

Ronny Purba [a,*], Michel Bruneau [b]

[a] Department of Civil Engineering, University of Minnesota, Duluth Campus, Duluth, MN 55812, United States
[b] Department of Civil, Structural and Earthquake Engineering, University at Buffalo, Amherst, NY 14260, United States

ARTICLE INFO

Article history:
Received 16 June 2014
Revised 18 February 2015
Accepted 3 April 2015

Keywords:
In-span plastic hinge
Experimental investigation
Seismic behavior
Steel plate shear walls
Cumulative plastic incremental deformation
Special moment connections
Finite element model

ABSTRACT

A cyclic pushover test of a three-story steel plate shear wall (SPSW) specimen was conducted to investigate the seismic behavior of this system when plastic hinge was predicted to develop along the span of horizontal boundary elements (HBEs). The experiment demonstrated that the in-span plastification caused a significant accumulation of plastic incremental deformations of HBEs. It also allowed to experimentally verify that moment–rotation hysteresis curves of HBE connections in SPSWs are not symmetric, but rather lopsided toward one direction, unlike that of special moment-resisting frames. Several of special moment connections experienced fractures, which is attributed to a higher rotation range prior to fracture of those connections. A finite element investigation of the tested specimen showed similar overall behavior to that observed during the experiment.

1. Introduction

Steel plate shear walls (SPSWs) have been known as an effective system to resist lateral loads and have been implemented in many buildings to provide ductile seismic resistance. Over fifteen implementations of unstiffened SPSWs in Canada, the USA, and other countries can be found in Sabelli and Bruneau [24] and Bruneau et al. [7]. The system typically consists of unstiffened steel infill plates connected to the surrounding beams and columns (a.k.a. horizontal boundary elements (HBEs) and vertical boundary elements (VBEs), respectively). The main advantage of SPSW system that contributes to its progressively more widespread acceptance is the significant stiffness and strength they can provide to buildings compared to other lateral force resisting systems. Many publications (e.g., [24,7]) have provided an extensive review on the historical development of SPSWs, the design philosophy and modeling of SPSWs, the analytical and experimental studies conducted by many researchers over several decades, and the codification of SPSWs (e.g., [1,8]).

Furthermore, experimental investigations have resulted in a relatively broad understanding of the fundamental behavior of SPSWs, investigating overall behavior of the system, ductile connection of infill plates to the surrounding boundary frame, behavior of infill plates, needed modifications of infill plate properties to reduce demand on boundary frame from yielded infill plates, connections between boundary elements, effective ways to increase the strength and rigidity of VBEs, and SPSW performance under various loading protocols ([23,13,22,16,5,25,9,11], to name a few). While validation of satisfactory cyclic performance has been reported, further research is still needed to advance the current understanding of the system in ways that might improve the available design procedures. For example, AISC seismic provisions [1] requires that HBEs and VBEs be designed to remain essentially elastic under the maximum tension forces from the yielded infill plates, except for plastic hinging at the ends of HBEs which is permitted. Implicitly, this indicates that in-span plastic hinges should be avoided. Whether or not in-span hinging is acceptable has been a contentious issue, particularly in the absence of factual data to support either position.

Recently, Purba and Bruneau [19] conducted an analytical investigation on the impact of plastic hinges that develop along the span of HBEs (a.k.a. in-span hinges) on the seismic behavior of SPSWs. The researchers reported that significant consequences of such in-span hinging included lower lateral strength due to partial yielding of the infill plates, significant plastic vertical deformations on the HBEs that incrementally accumulated as the structure was pushed cyclically (defined as "plastic incremental deformations"), and greater HBE rotation ranges/demands. While that

* Corresponding author.
E-mail addresses: rhpurba@d.umn.edu (R. Purba), bruneau@buffalo.edu (M. Bruneau).

http://dx.doi.org/10.1016/j.engstruct.2015.04.008
0141-0296/

research has established the potential consequences of developing in-span hinges, an experimental program was deemed desirable to investigate whether the reported undesirable behaviors could also be observed in an actual SPSW.

This paper presents the results of a cyclic pushover test of a three-story SPSW specimen designed with the expectation of developing in-span plastic hinging. This experiment was intended to investigate whether in-span HBE plastic hinging actually occurs in actual SPSW, or if this was just an artifact of unavoidable simplifications in numerical models. In addition, this specimen was instrumented such as to attempt quantifying possible accumulation of plastic incremental deformations on the HBEs and partial yielding of the infill plates. This experimental program also aimed (in a limited way) to assess the performance of special moment resisting connections in such SPSWs. The paper ends with a discussion on the effectiveness of a finite element model developed to simulate the experiment.

2. Design of 3-story SPSW specimen

The three-story SAC model building with a plan dimension of 120 feet by 180 feet and a typical story height of 13 feet (FEMA 355-C) [14] was selected as a prototype for this research; it is located on Class B soil in downtown Los Angeles and representative of an office building. In this study, two single-bay SPSWs act as the primary lateral load resisting system. Located on the building perimeter in the North–South direction, each one of them was assumed to carry seismic loads corresponding to an effective seismic weight equals half of the 6504 kip total weight of the structure. For simplicity, design of a 1/3-scaled three-story single-bay SPSW specimen was not conducted at the prototype level, but rather directly at the specimen level.

The resulting geometry of the SPSW specimen has a typical story height of 52 in. and a bay width of 120 in. However, due to dimensional restrictions of the gravity column system (as later explained) available in the Structural Engineering and Earthquake Simulation Laboratory (SEESL) of the University at Buffalo, as well as to minimize design differences with another research project conducted in parallel to this study [12], the final specimen dimensions were slightly modified to have and average story height of 51 in. and a bay width of 90 in. An analytical investigation detailed in Purba and Bruneau [20] ensured that the intended specimen behaviors with this modification could still be observed during the experiment. The total effective seismic weight for the specimen was equal to 361 kips.

The Indirect Capacity Design method for SPSW provided in the commentary of the AISC Seismic Provisions [1] was followed when designing the specimen. On the basis of the spectral acceleration maps in the FEMA 450 provisions [15], the design short and one-second spectral ordinates, S_{DS} and S_{D1}, for the site where the prototype is located were 1.3 g and 0.58 g, respectively. Using the fundamental period of the specimen T of 0.13 s, a response modification factor R of 7, and an importance factor I of 1, the total design base shear V to be resisted by the specimen was 65 kips. Using Eq. 12.8-11 in the ASCE 7-10 documents [3], the equivalent lateral loads along the height of the specimen were 32, 22, and 11 kips from the third to the first floor. These story forces were resisted entirely by infill plates without considering the contribution to lateral strength provided by the surrounding boundary frames.

As shown in Fig. 1a, the overall height of the specimen from its base to the top of column was 160 in. and the width of the specimen measured between the outer flanges of the East and West columns was 96.75 in. The steel plates used for the first, second, and third floor panels were 13-gauge (0.0897 in.), 14-gauge (0.0747 in.), and 19-gauge (0.0418 in.) plates, respectively. W8×13 and W6×12 were selected for the bottom and top anchor beams (i.e., HBE0 and HBE3) while S5×10 was selected for the intermediate beams (i.e., HBE1 and HBE2). In addition, W6×25 was selected for the columns (i.e., VBE1 to VBE3). The average material properties of each component from a total of 27 tensile coupons are summarized in Table 1.

Special moment resisting connections [i.e., Welded Unreinforced Flange-Welded Web (WUF-W) connection specified in the AISC 358-10 documents [2]] were designed for all HBE-to-VBE connections, even though AISC 341-10 [1] only requires ordinary moment resisting connections for the HBEs of SPSWs. This was done because significantly greater plastic rotations are expected at the ends of HBEs when in-span hinging is allowed to develop [19]. A limited ultrasonic and phase array test was conducted on several connections to ensure the quality of the CJP Groove welds on the specimen. It is important to note that, due to scaling issues, not all AISC 358-10 [2] prescribed limits and details for prequalified WUF-W connection were respected in designing the connections of this 1/3 scaled specimen. For example, a W6 column was used, which is shallower than the pre-qualified W12 or W14 column. Likewise, the weld access hole was smaller than the minimum dimensions specified in the AISC 358-10 [2]. While results from this study still provide useful information, full-scale testing may be desirable to validate findings and recommendations obtained from the behaviors of the 1/3 scale connections used in this study. Details of the specimen design can be found in Purba and Bruneau [20].

3. Experimental setting

The specimen was positioned in the East to West direction and anchored to an existing floor plate (1.5 in. thick, 9 ft. by 12 ft. dimension) using thirteen ¾ in. diameter A490 high-strength slip-critical bolts on each column base plate (1 in. thick with 14 in. by 12 in. foot print), capable of transferring the plastic moment capacity of the columns. The existing floor plate was anchored to the 24 in. thick concrete strong floor using 22 high strength tension rods (i.e., F_y = 130 ksi; F_u = 150 ksi) of $1^1/_8$ in. diameter, with a corresponding tributary area of 24 in. by 24 in. per rod.

A gravity column system was used to apply loads and provide lateral supports to the specimen [17]. As shown in Fig. 1b, the gravity column system sandwiches the SPSW specimen and is fitted with supports to prevent lateral torsional buckling of the beams. The angles connecting the gravity mass to the specimen (Fig. 1c) served both to provide out-of-plane lateral support and as a load transfer mechanism. In addition, three angles at the bottom side of the gravity mass were added to laterally brace the beam bottom flanges (Fig. 1d). Lateral supports were also added at the column locations both on the top and bottom sides of the gravity mass (Fig. 1e). Furthermore, lateral supports for the bottom anchor beam (HBE0) were welded to the floor plate, where two WT3×4.5 sandwiched the beam at its mid-point. To reduce friction between the specimen and its lateral supports, 1/8 in. thick polytetrafluoroethylene (PTFE) sheets were used on each angle-to-angle and angle-to-specimen surfaces. The specimen was instrumented to collect experimental data, including displacement transducers (i.e., string pots and Krypton sensors), uniaxial and triaxial Rosette strain gauges, load cells, and video cameras. Details of the instrumentation can be found in Purba and Bruneau [20].

Lateral loads generated by actuators were directly applied to each floor's rigid mass plates, which afterward transferred loading to the specimen via twelve ¾ in. diameter A325 high-strength bolts (six per mass plate), using three connection angles on each side of the specimen (and two bolts per angle). These bolts were

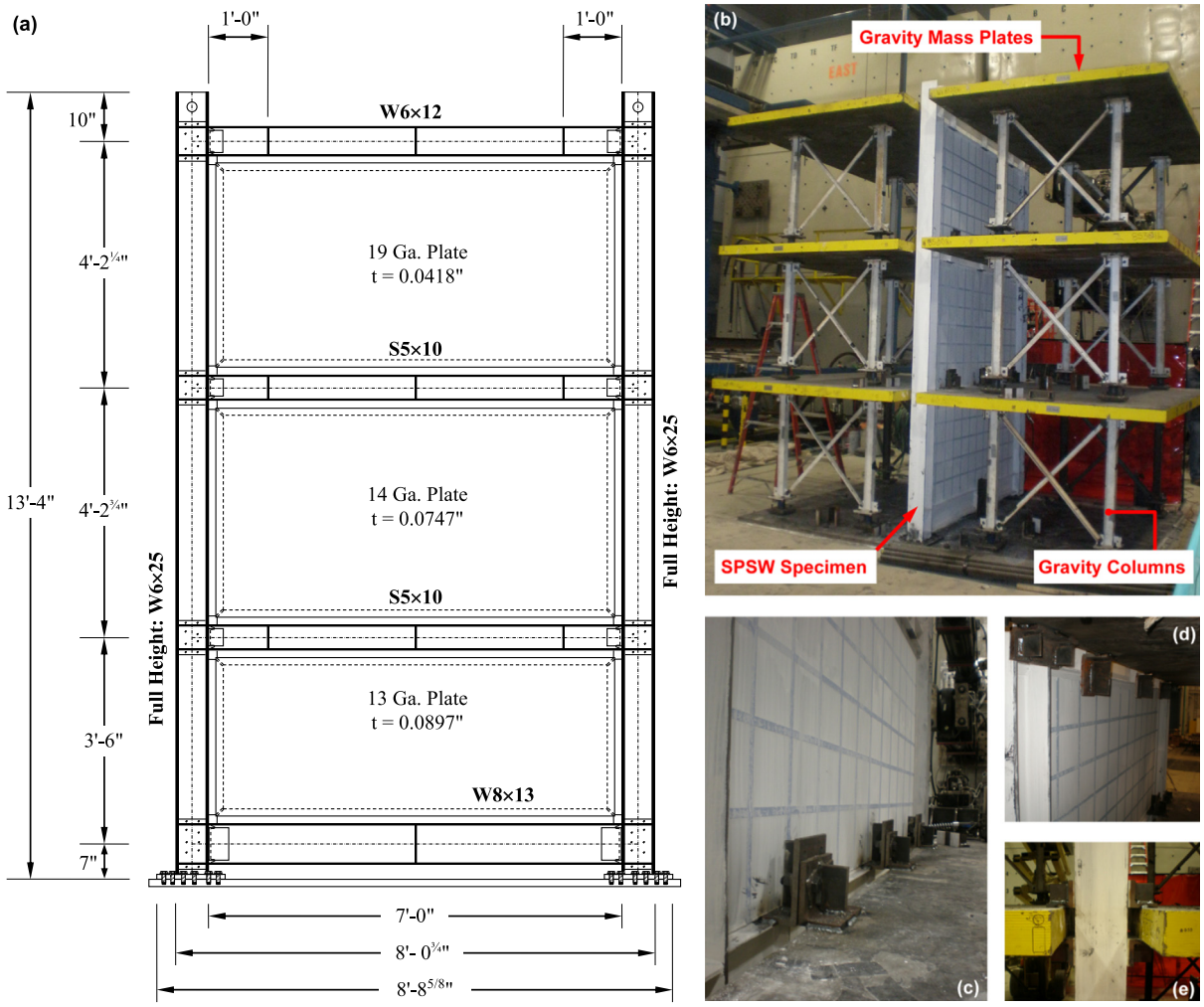

Fig. 1. Three-story SPSW specimen: (a) elevation view; (b) experimental setup with gravity column system; (c) angles for load transfer mechanism; (d) and (e) angles for lateral supports at HBE bottom flange and both sides of VBEs.

Table 1
Summary of material properties from tensile coupon test.

Component	Nominal thickness (in)	Actual thickness (in)	Modulus of elasticity (ksi)	Yield strength (ksi)	Ultimate strength (ksi)	Rupture strain (%)
Plate GA13	0.0897	0.0886	28,420	26.668	45.933	39.31
Plate GA14	0.0747	0.0713	27,736	23.598	42.292	46.29
Plate GA19	0.0418	0.0402	26,772	20.034	39.270	42.58
W6×25 Web	0.320	0.3458	33,522	52.875	65.664	33.97
W6×25 Flange	0.455	0.4322	32,136	52.475	66.768	34.27
W6×12 Web	0.230	0.2268	34,473	52.775	64.460	36.65
W6×12 Flange	0.280	0.2799	29,441	52.350	63.776	33.64
S5×10 Web	0.214	0.2028	30,323	49.975	70.521	27.85
W8×13 Web	0.230	0.2360	24,080	54.200	66.175	32.98
W8×13 Flange	0.255	0.2405	30,126	50.805	62.222	31.22

W6×25 = VBE, W6×12 = HBE-T, S5×10 = HBE-I, W8×13 = HBE-B.

capable of transferring twice the maximum actuator forces of 66 kips that was expected to develop at 5% drift (to provide a desirable experimental margin of safety). Each bolt was snug-tightened in 3-in. long vertically slotted holes (Fig. 1c). While downward movements of the beams were expected to be 1.25 in. at 5% drift, the connecting angles with overlapping slotted holes theoretically allowed a maximum 5.25 in. downward movements of the beams while the frame was cycled laterally in the East and West directions.

One MTS dynamic actuator at each floor, capable to deliver 100 ton payloads and 40 in. strokes was used in this experiment. The third story actuator was set up in a displacement-control mode, while the other two actuators were in a force-control mode. In other words, the first and second story actuators were slaved to the third story actuator which acted as the master actuator and underwent a specified cyclic displacement history. The amount of forces applied by the first and second story actuators to the specimen at a particular time step respectively were 1/3 and 2/3 of the

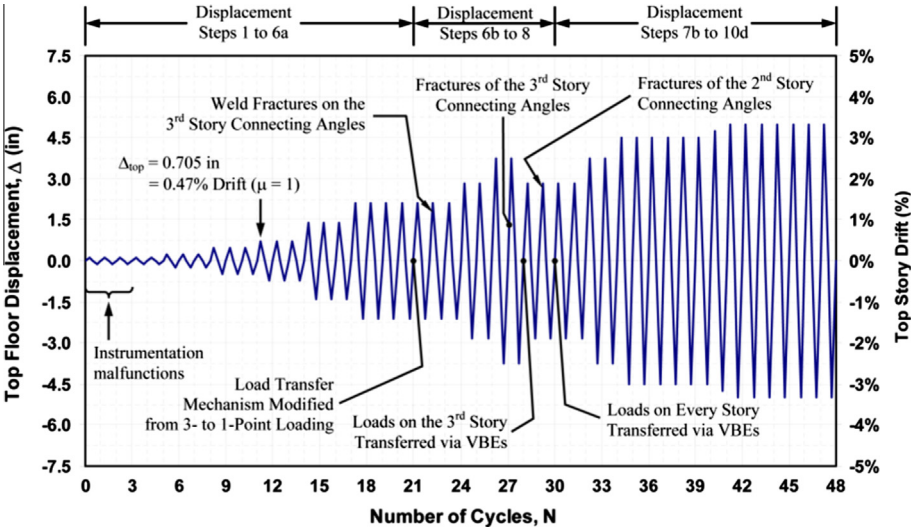

Fig. 2. Cyclic displacement loading history.

forces recorded in the third story actuator within the previous time step.

The loading protocol for this experimental program was developed as a combination of the ATC-24 protocol [4] and the AISC Seismic Provisions [1] requirements. Specifically, the first half of the loading protocol followed the loading sequences specified in the ATC-24 formulated as a function of ductility ratio (μ), defined here as the ratio of top story displacement (Δ_3) to the specimen effective yield displacement (δ_y), while its second half followed the AISC requirements that are in terms of top story drift. The specimen effective yield displacement was determined as the point where the elastic and inelastic tangents intersected to each other on a force–displacement pushover curve of the specimen analytical model. Here, the resulting top story displacement was 0.705 in., corresponding to a drift of 0.47%. A complete cyclic displacement loading history for this experimental program is graphically shown in Fig. 2 with a total of 10 displacement steps and a cumulative 48 cycles applied to the specimen.

4. Experimental observations

4.1. Displacement Steps 1 to 6a

The first part of the experimental program consisted of a cumulative 21 cycles with a target maximum displacement at the top story (called here the "actuator displacement") gradually increased from 0.12 to 2.12 in. (i.e., corresponding to ductility ratio increased from $^1/_6$ to $3\delta_y$ or top story drift from 0.08% to 1.41%). As expected, elastic buckling of the infill plates and practically linear force–displacement relationship was observed during several early displacement steps. Noticeable signs of yielding were observed when the specimen reached an expected effective yield displacement of 0.71 in. (=0.47% drift) in displacement Step 4. Flaking of whitewash was noted around the bases of both columns but did not occur on the infill plates despite the fact that the permanent buckling of the infill plates was more pronounced in this step than in the previous steps. A residual top story displacement of approximately 0.08 in. was recorded at the end of displacement Step 4. During displacement Step 5, at $2\delta_y$ (=0.94% drift), flaking of whitewash appeared predominantly on the second story infill plate and at several spots on the first story infill plate. Yielding around the bases of columns spread to a larger area. Yield lines were visible on the flanges and web of HBEs. No tearing on the infill plates was found yet. Within displacement Step 6 ($\Delta_3 = 3\delta_y = 1.41\%$ drift), yielding at those aforementioned locations spread to an even larger area.

Several interesting behaviors were observed within this first experimental stage. The base shear value was increasingly higher than the estimated base shear for the applied top story displacement, yet the HBE vertical displacements were significantly lower than that was expected. By the time a top story drift amplitudes of 1.41% was reached, the maximum base shear obtained was 34.3 kips higher than the estimated value from a SAP2000 analysis using a strip model of the specimen (i.e., 145 kips versus 110.7 kips). Incidentally, the strip model consists of series of tension-only strips to simulate post buckling behavior of unstiffened steel panels; these strips are typically of equal width and pin-connected to the surrounding boundary frame which is modeled with conventional beam element. Details about the strip model can be found in other publications (e.g., [1,24]).

Furthermore, HBE3 and HBE2 theoretically should have deformed downward by approximately 0.43 in. However, the actual maximum deformation on these HBEs was no more than 0.20 in. This smaller value in the HBE vertical deformations suggested that the accumulation of plastic incremental deformations on the HBEs was not as pronounced as originally predicted. However, a concentration of yield lines was observed on the inner side of the HBE top flange below where the load transfer angles were welded; it was speculated that the high-strength bolts used in the connecting angles to transfer actuator loads from the gravity mass plate to the specimen might have been stuck and that, as a consequence, the HBEs were not completely free to move vertically. Such unintended restraints would have also explained the observation that the specimen behaved more rigidly than anticipated by designed, as additional forces beyond what was expected would have been required to push the specimen to the specified displacement target. A more intriguing behavior at this stage was the increasing differences between the actuator displacement and the top story specimen displacement (called here the "wall displacement"). When the level 3 actuator pushed and pulled the specimen to the 2.12 in. target in displacement Step 6 ($\Delta_3 = 1.41\%$), the specimen only moved by 1.93 and 1.12 in. in the West and East excursions, respectively.

In light of these persisting differences between predicted and experimentally obtained behaviors, the experiment was temporarily stopped. After careful review of experimental data and

some additional analyses to better model the load transfer mechanism provided by the angles, several adjustments to the experimental setting were introduced. First, because it was believed that the multiple connection points along the HBE were "fighting each other" and effectively restraining beam rotations needed for experimental behavior to match the predicted one, bolts at the quarter- and third quarter-span of every HBE were taken out, leaving only 4 bolts at the mid-span of each HBE to transfer actuator forces to the specimen (the A325 bolts previously used were replaced by higher strength A490 bolts of the same ¾ in. bolt diameter). Second, string pots were added to measure the difference in horizontal displacements between the actuator and the mid-span point of each HBE in an attempt to study the cause for the significant difference between the actuator and wall displacements. Third, because video feeds indicated uplifts at the East and West columns, displacement transducers were added to their bases to monitor uplifts at those points.

4.2. Displacement Steps 6b to 8

With the adjusted setting, the experimental program resumed with a cumulative 9 cycles at target displacements gradually increased from 2.12 to 3.75 in. (i.e., Δ_3 = 3 to 5.32δ_y = 1.41–2.5% drift). Here, the mid-span connecting angles were able to substantially slide along the vertically slotted holes, which facilitated the downward movement of HBEs as lateral loading progressed. However, significant difference between the actuator and wall peak displacements remained noticeable. For example, at a peak displacement target of 2.82 in., the differences between the actuator and wall displacements were 0.98 and 0.53 in. during the West and East excursions, respectively. The recorded data (measuring the displacement between the actuator and the mid-span point of HBE3) confirmed that axial deformations along the HBE3 were not responsible for this significant discrepancy. Instead, it was significant rotation of the mid-span connecting angles that mostly accounted for this discrepancy. In other words, some of the lateral displacements imposed by the actuators rotated the connecting angles, resulting in lower lateral displacements experienced by the specimen compared to actuator displacement. Significant cyclic rotations experienced by these connecting angles lead to their low cycle fatigue fractures at the top floor in Step 8 at 2.5% top story drift (=5.32δ_y), and on the second floor soon after.

To repair the specimen and provide a more direct load transfer mechanism via the columns, two MC6×16.3 channels and L6×4×½ steel angles were welded to connect the mass plate to both sides of each column at the third and second floor. A similar steel angle connection was installed for the first story load transfer mechanism even though fracture did not occur there.

4.3. Displacement Steps 7b to 10d

Having the new loading transfer mechanism installed, it was considered necessary to repeat the previous two displacement steps (with two cycles each) to ensure the effectiveness of this final mechanism transferring loads to the specimens. Compared to what occurred in the previous two displacement steps, here yielding in all the previously reported locations essentially spread to larger area. This can be understood because now the wall displacement was actually significantly larger, and for the first time, equal to the actuator displacement. In addition, vertical deformations of the HBEs significantly increased (e.g., the maximum values recorded in Step 8a were 0.75 and 0.59 in. for HBE3 and HBE2, respectively, which were comparable to the estimated values). Minor infill plate tearing and HBE in-span plastification (Fig. 3) were observed for the first time in Step 8a.

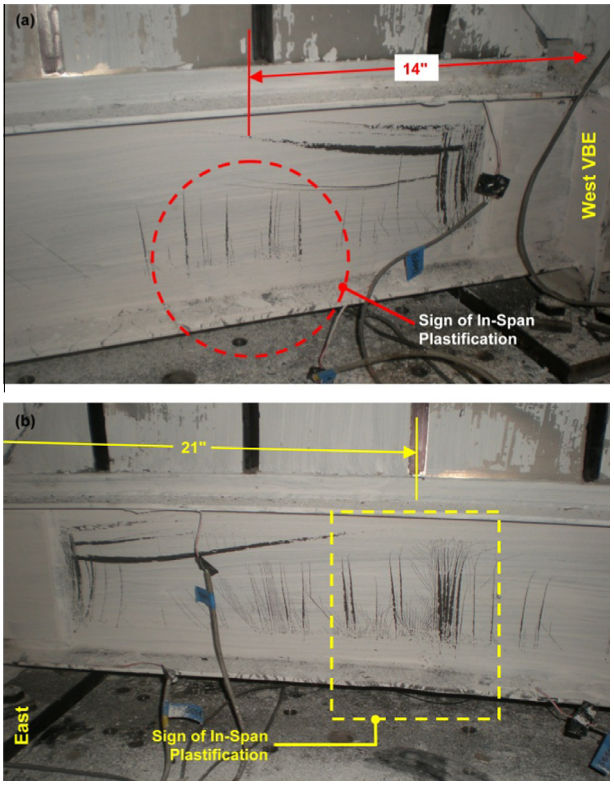

Fig. 3. Sign of in-span plastification on HBE3 during displacement Step 8a (Δ_3 = 2.5% drift = 5.32δ_y): (a) West side; (b) East side.

As the hysteretic curve showed no strength degradation, the experimental program continued with two cycles at the higher target displacement in Step 9 (i.e., Δ_3 = 3.0% drift = 6.38δ_y). The resulting peak base shears when cycling at 3.0% drift amplitude were 166.9 and 180.6 kips for the West and East excursions, respectively. Cracks in the infill plates, approximately 0.5 in. long, were observed on the first and second story infill plates. Lateral torsional buckling (LTB) and flange local buckling were observed at the location of in-span plastic hinge at HBE0 (Fig. 4).

Relatively small gaps between the steel floor plate and the concrete strong floor were observed at the SPSW column locations. These residual uplifts at the East and West column locations were 0.17 and 0.01 in., respectively (when the specimen reached its target displacement, column uplifts were 0.57 and 0.65 in. at the same respective locations). In an attempt to prevent further permanent of uplifts and damage to the floor plate, four additional cycles at the same displacement target of 3.0% top story drift were applied, in the expectation that strength degradation of the specimen would occur under this repeated loading (i.e. resulting in lower maximum base shear and lower uplift forces in the SPSW columns). The resulting peak base shears were 18.4 and 21.1 kips less than that in displacement Step 9 for the West and East excursions, respectively. The residual uplifts remained at the same magnitude while the maximum uplifts slightly reduced. The infill plate crack grew to approximately 1.5 in. long in the first story.

While closely monitoring floor plate uplifts and peak base shear, the experimental program then continued to higher displacement targets of 3.17 and 3.3% drift (=6.74 and 7.09δ_y, respectively) for 8 cumulative cycles. Here, the peak base shears reached in displacement Step 9 were never reached again; maximum and residual uplifts recorded at both East and West column locations remained approximately the same as that in the previous steps. Fractures were observed at the WUF-W flange connections at

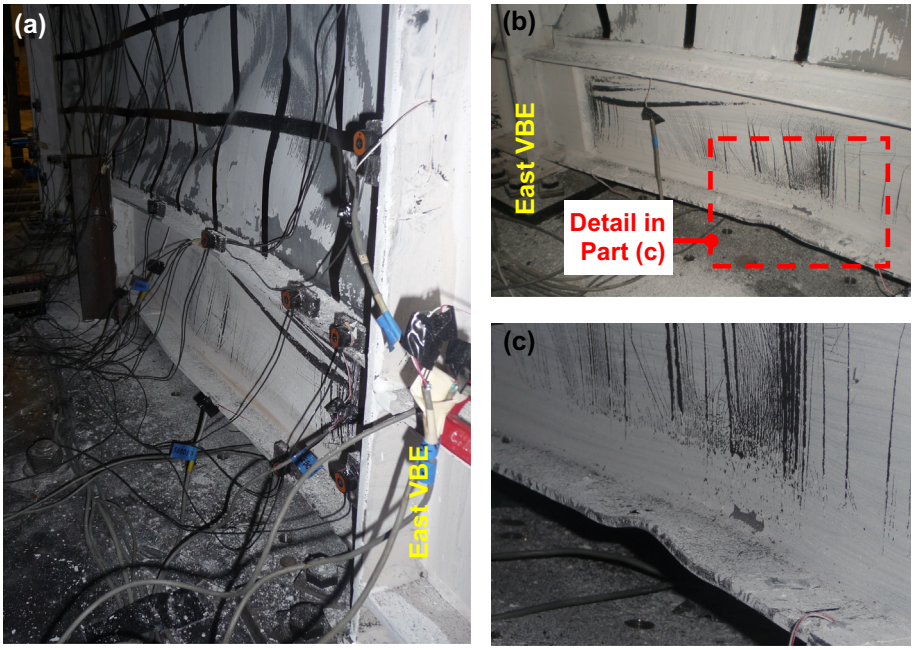

Fig. 4. Specimen condition at displacement Step 9 (Δ_3 = 3.0% drift = 6.38δ_y): (a) lateral torsional buckling (south view); (b) and (c) flange local buckling (north view).

HBE1 and HBE2 (Fig. 5a–c) and a minor weld crack was observed on the West VBE connection to its base plate (Fig. 5d). In addition, plate tearing was noted at several new locations on the first and second stories.

After the displacement Step 10d cycles of 3.3% target drift, the test was stopped for several reasons, namely: (1) the specimen practically exhibited the same behavior within the last several displacement steps and no new events would have been observed if cycles at the same displacement targets had been further repeated; (2) it was judged prudent to not push the specimen beyond the current displacement target to prevent damage to the floor plate; (3) there was a concern that because the lower two floor actuators were acting in a force control mode, extreme damage to the specimen at the first or second story could lead to an

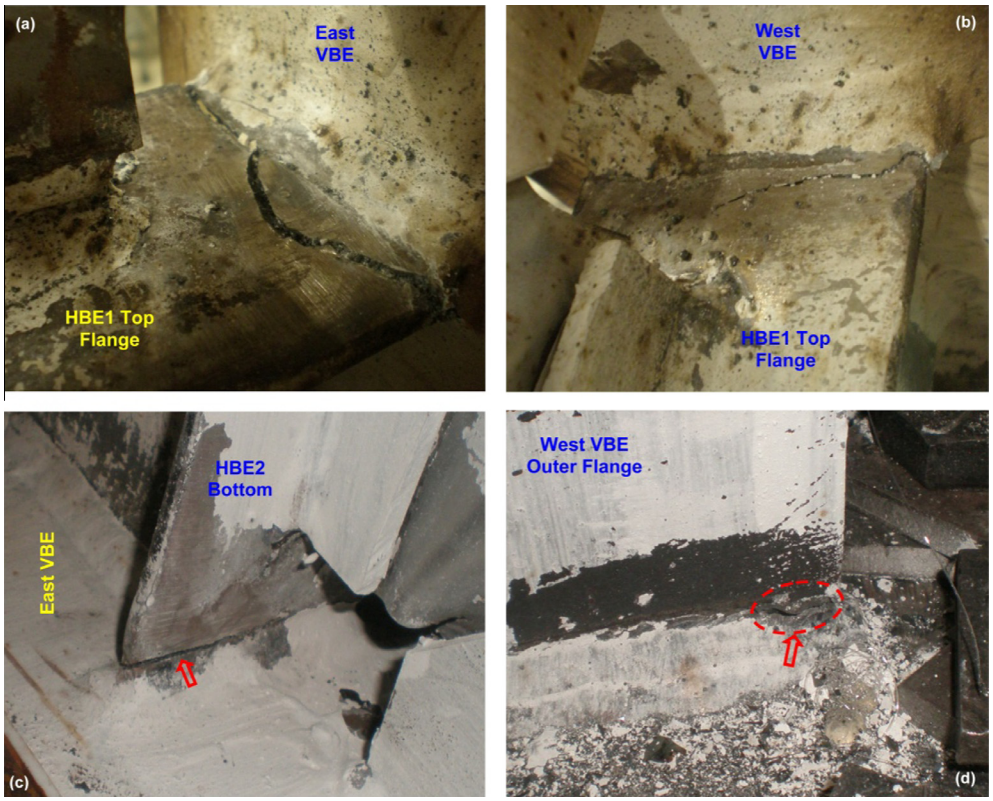

Fig. 5. Special-moment resisting connection fractures in displacement Step 10c (Δ_3 = 3.33% drift = 7.09δ_y): (a) and (b) HBE1; (b) HBE2; (c) West VBE.

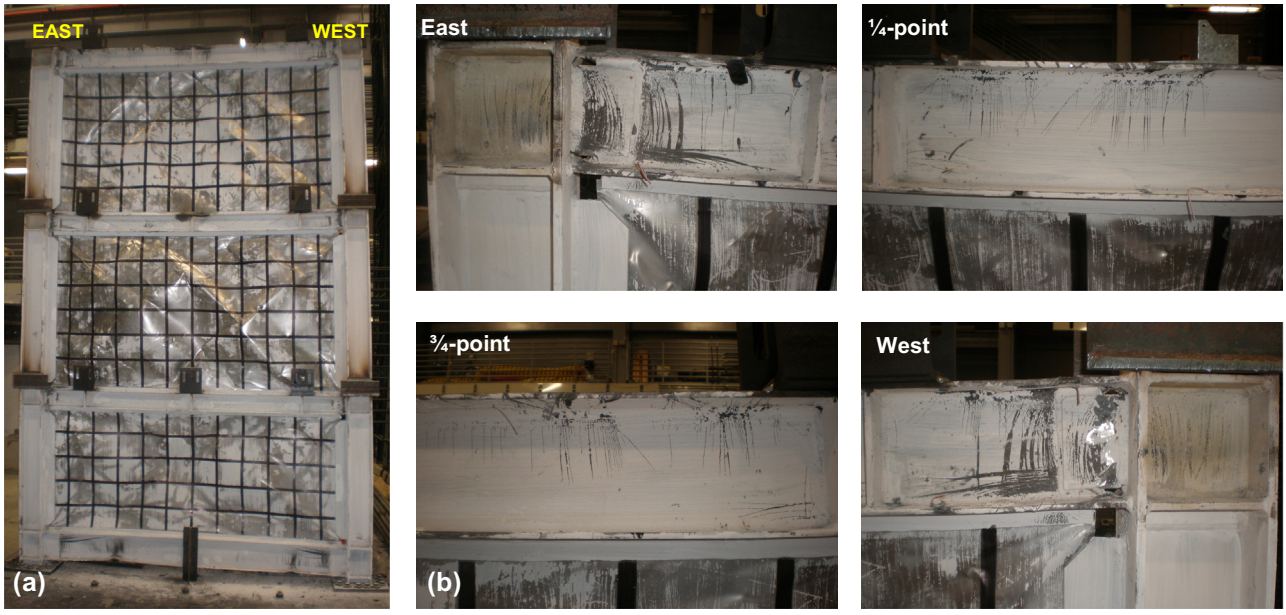

Fig. 6. Specimen final condition: (a) overview; (b) details of HBE3.

uncontrolled behavior, resulting in an unexpected collapse and damage to the laboratory equipment (i.e., preventing in-situ repairs of damage and other possible fixes to the test set-up).

The specimen final condition is shown in Fig. 6. With removal of the gravity column system, additional inelastic evidence could be observed that had not been noticed during testing: (1) sign of in-span plastification was also observed on HBE3 (Fig. 6b); (2) another flange fracture was observed at the HBE1 connection to the West VBE (Fig. 5b). Maximum residual deformations for top to bottom HBEs were 0.75, 0.5, less than 0.25, and 0.875 in., respectively; and permanent out-of-plane displacement of HBE0 at the location where LTB occurred was 1.5 in.

5. Discussion of experimental results

Hysteretic plot of the base shear versus top story displacement hysteresis is presented in Fig. 7. In general, the hysteretic loop resembles that expected for unstiffened thin SPSWs reported in past experimental research (e.g., [13,25,9]), namely: exhibiting pinching in the hysteretic curve, stable and ductile behavior when undergoing large lateral drifts, and relatively small strength degradation between cycles at the same displacement step. Numerous

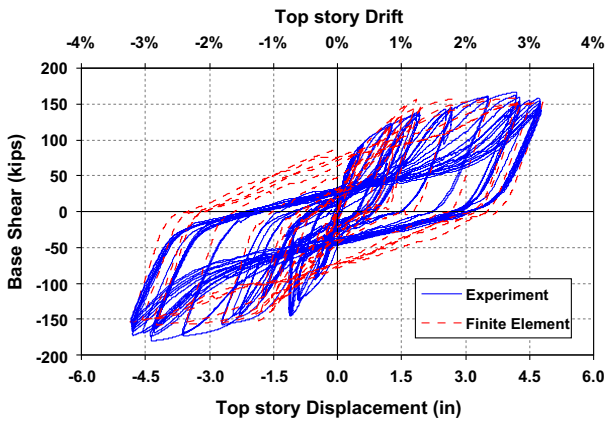

Fig. 7. Base shear versus top story displacement.

studies investigating the seismic response of SPSW have reported that the pinching of the hysteretic curves, by itself, is not detrimental on the seismic response of SPSWs (e.g., [6,21]). Specific to this experiment, strength degradation beyond the maximum story shear was not observed because the experimental program was concluded before that behavior could substantially develop.

Inspection of the specimen after the test (Fig. 6) showed that plastic hinges developed at both ends of each HBE and at the base of each VBE. While it was not as pronounced as that on HBE3 (Figs. 3 and 4), evidence of in-span plastic hinge was also observed on HBE3 indicated by yielding initiated at its top flange and spread to its web around the ¼- and ¾-points (Fig. 6b). Moreover, yield lines distributed along HBE flange indicated that plastification of the upper two HBEs was not localized within a finite length as in the case of HBE0 but rather distributed within a longer span. Qualitative indication suggested that complete infill plate yielding occurred in each panel as shown by flaking of whitewash roughly over the entire surface of each panel. However, quantitative measurements indicated that plate yielding did not develop simultaneously, but rather progressively. In-span plastification of HBE contributed to this delay of plate yielding. At the conclusion of the test, it appeared that the entire infill plates had yielded. Hence, the theoretically predicted incomplete yielding of the infill [19] seems to not have happened. However, it is important to emphasize that the initial load transfer set-up used in the first part of the experimental program is partly responsible for this difference in behavior, especially at the upper infill plates. When vertical movements of the upper two HBEs were limited, infill plates adjacent to the panel corners could elongate beyond their yield displacements.

Recorded vertical deformations during this cyclic pushover testing are presented in Fig. 8a for HBE3, HBE2 and HBE0. Although evidence of in-span plastic hinge (inferred from yield line in the whitewash) was only clearly visible on HBE0, the results in those figures indicate that accumulation of plastic incremental deformations were apparent not only on HBE0 but also on HBE2 and HBE3. The "backbone" displacements (defined as HBE vertical displacement when the structure reached the maximum target drift of every cycle) progressively increased from practically zero in the first displacement step to 1.64, 0.76, and 1.11 in. respectively for HBE0, HBE2, and HBE3 when the specimen was cycled up to

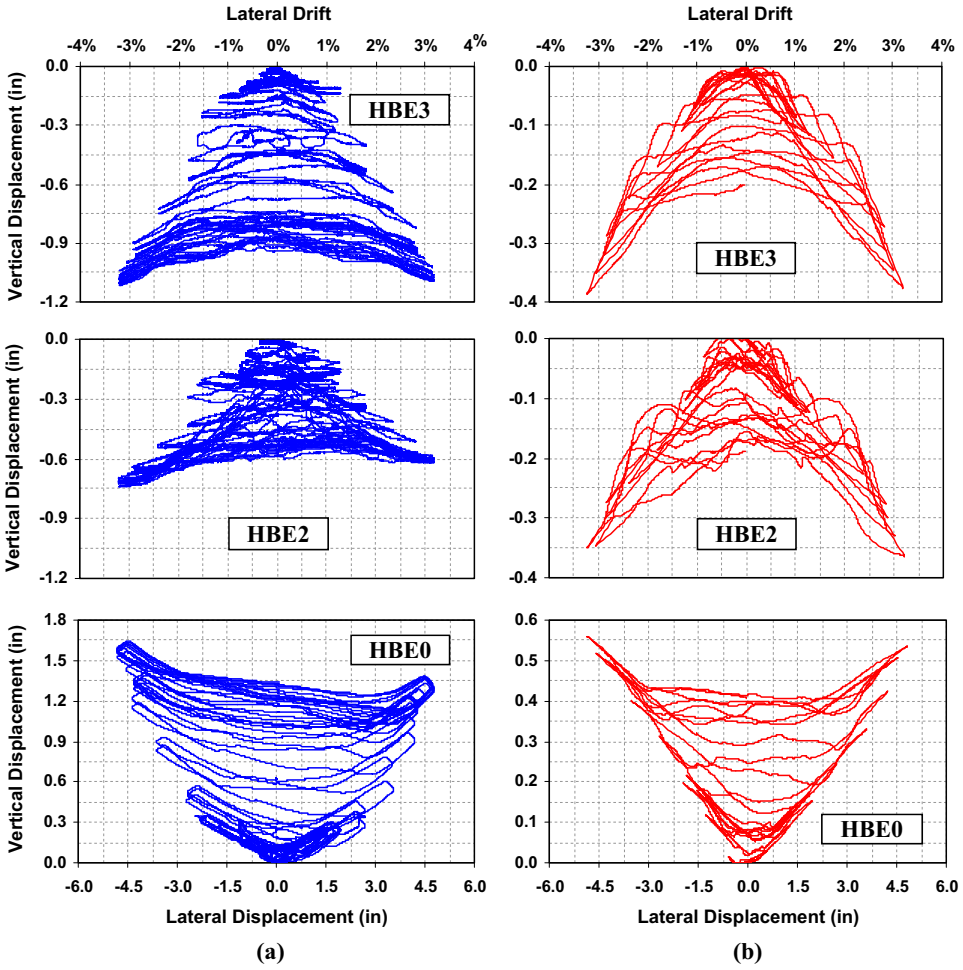

Fig. 8. HBE vertical displacement structure versus lateral displacement (a) experiment; (b) finite element analysis.

3.33% top story drift amplitude. The same trend was also observed on the progression of the "residual" displacement (defined as HBE residual vertical displacement when the structure returned to its original position at 0% drift).

The accumulation of plastic incremental deformations predominantly occurred in the third part of the experimental program (i.e., displacement Steps 7b to 10d) after the load transfer mechanism was modified to ensure development of the HBE vertical movement. For example, approximately 57% of the maximum backbone displacement of HBE3 obtained at the end of the test occurred within the last 18 cycles. Note that plastification of HBE3 due to rotation of the load-transfer mid-span connecting angles influenced its vertical deformations (Fig. 8a), but the actual contribution of this effect to the total HBE3 plastic deformations was difficult to quantify.

A number of Krypton sensors had been installed around the perimeter of the first story panel. Data from those sensors allows observation of HBE0 and HBE1 vertical deformations along their spans as the cyclic load progressed. Fig. 9 shows deformation profiles of HBE0. Krypton sensors recorded somewhat the same deformations at every point along the HBE span within displacement Steps 1a to 6. Once that HBE became completely un-restrained (i.e., Steps 7b to 10d), the HBE deformation profiles changed significantly.

Purba and Bruneau [19] reported that the moment hysteresis curves of HBE connections in SPSWs are not symmetric, but rather lopsided toward one direction when subjected to a symmetric cyclic displacement history, unlike like that of special moment-resisting frames (and other lateral load resisting systems) that exhibit symmetric hysteretic curves (i.e., with equal positive and negative rotations developing under symmetric displacement history). The experimental results shown in Fig. 10 for HBE3 and HBE2 confirm the development of such un-symmetric hysteretic curves, making it possible to experimentally verify this analytically predicted behavior. Note that unidentified factors contributed to some irregularities in the hysteresis curves of HBE3 in its earlier cycles, introducing an early "drift" in the results, but this did not affect the subsequent one-sidedness behavior of the moment–rotation hysteretic loops.

Table 2 presents the maximum rotations and "rotation ranges" recorded for HBE3 and HBE2 at their connections to the West VBE and compared them to their corresponding analytical results. Here, rotation range is defined as the absolute difference between rotations at the positive and negative extremes of one particular displacement step/cycle (a.k.a. rotation demand). Although the predicted HBE3 maximum rotation is comparable to that obtained from the experimental program, their rotation ranges were somewhat different. When the specimen was cycled up to the maximum target drift of 3.33% within the last displacement step, HBE3 maximum rotation reached 0.054 radians compared to 0.052 radians obtained from the cyclic pushover analysis. However, the recorded HBE3 rotation range was 0.031 radians compared to the analytical value of 0.042 radians. In contrast, the predicted HBE2 maximum rotation and rotation range were 0.015 and 0.01 radians higher than their respective actual values recorded during the experimental program.

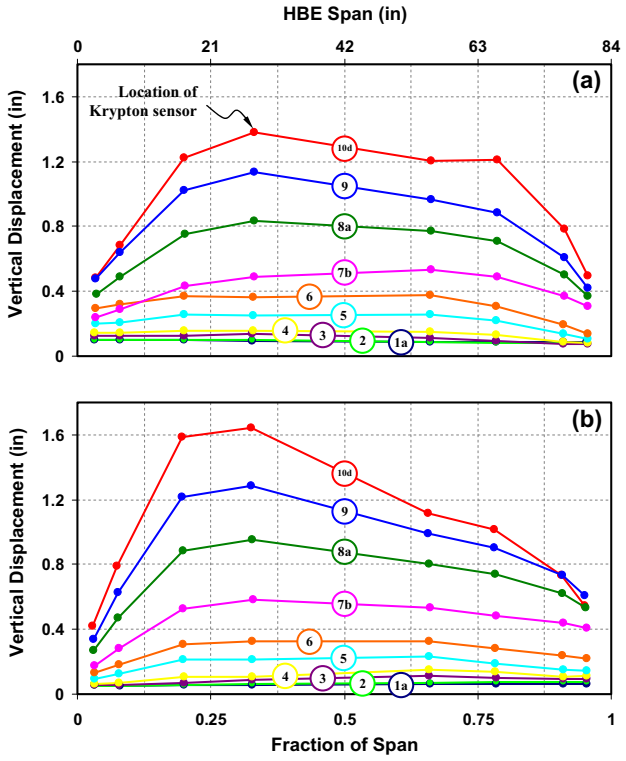

Fig. 9. Profile of HBE0 vertical displacement: (a) West excursion; (b) East excursion.

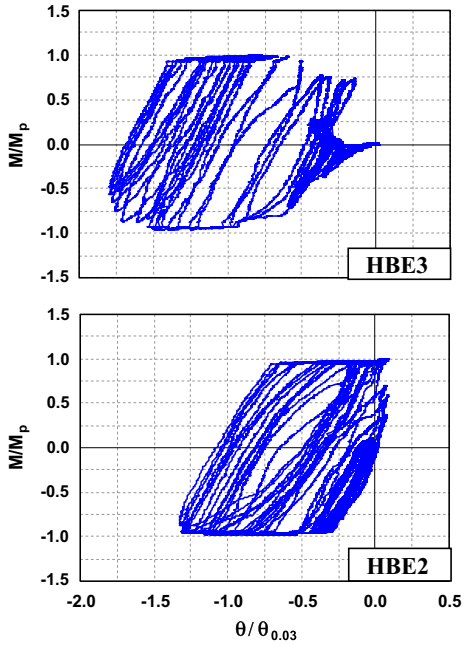

Fig. 10. Normalized moment rotation hysteresis.

In spite of higher maximum rotation recorded at HBE3 compared to that of HBE2, HBE3-to-VBE3 special moment connections remained intact up to the conclusion of the experimental program. In contrast, HBE2 which experienced lower maximum rotation suffered connection fracture at its connection to the VBE2. The significantly higher rotation range recorded on HBE2 compared to that of HBE3 (i.e., 0.042 versus 0.031 radians within 3.3% drift cycle) is considered to have played an important role to the fracture of HBE2 connection.

Table 2
Maximum rotation and rotation range in HBE3 and HBE2.

HBE	Experiment result			Analytical result		
	θ_{max} at 3.3% drift	θ_{range} at 3.0% drift	θ_{range} at 3.3% drift	θ_{max} at 3.3% drift	θ_{range} at 3.0% drift	θ_{range} at 3.3% drift
3	0.054	0.023[a]	0.031[b]	0.052	0.032[e]	0.042[f]
2	0.040	0.034[c]	0.042[d]	0.055	0.043[g]	0.052[h]

Note: (Unit: radians).
[a] Rotation range: −0.014 to −0.037.
[b] Rotation range: −0.023 to −0.054.
[c] Rotation range: +0.002 to −0.032.
[d] Rotation range: +0.002 to −0.040.
[e] Rotation range: −0.010 to −0.042.
[f] Rotation range: −0.010 to −0.052.
[g] Rotation range: −0.004 to −0.047.
[h] Rotation range: −0.003 to −0.055.

6. Finite element investigation of tested spsw specimen

ABAQUS/Standard [10] was utilized to define a finite element model (FEM) of the specimen. A 7 ft. wide portion of the floor plate was explicitly included in the FEM developed (Fig. 11a). However, the concrete strong floor and the gravity mass frame were excluded. Fish plates and shear tabs were taken into consideration in the design and analysis of the specimen as they significantly affected the ultimate capacity of relatively small W-sections used for HBEs [20]. Hence, they were included in the FE model developed. The entire infill plate and boundary elements were meshed using the isoparametric S4R shell elements, a four-node doubly curved general-purpose conventional shell element with reduced integration and hourglass control. The resulting SPSW and floor plate finite element model contained 33,288 shell elements with an average dimension of 1 × 1 in. per shell element.

Taken as their test coupon values (Table 1), steel used for the boundary frame was comparable to that of a typical ASTM A572 Gr. 50 steel (F_y = 50 ksi, F_u = 65 ksi, Poisson's ratio v = 0.3) and the yield strengths of light-gauge steels were slightly below 30 ksi yield strength. An elasto-perfectly plastic material model was used to idealize the ASTM A36 steel (F_y = 36 ksi) used for the floor plate. To define the inelastic (hardening) behavior in boundary frame and infill plates, the *Combined Hardening* model was used. This hardening model is a nonlinear combination of *Isotropic Hardening* and *Kinematic Hardening* models. The Von Mises yield criteria was used.

In the experiment setup, the angles connecting the gravity mass to the specimen (Fig. 1c) served both to provide out-of-plane lateral support and as a load transfer mechanism. In the FE model however, these roles have to be separated to avoid conflict of constraints in several nodes (i.e., known as the *Overconstraint* condition in ABAQUS term). This was done by restraining the exterior nodes of HBE flange and stiffener elements at the locations of the angles against out-of-plane movement and assigning nodes at the centerline of HBE top flange (again at the angle locations) to transfer the load to the specimen. As for VBEs, the exterior nodes around the perimeter of panel zones (i.e., nodes of VBE flange and continuity plate elements) were restrained against out-of-plane movement and nodes at VBE web at the level of HBE top flange were selected to transfer the load. This approach also simplified the modeling process when considering changes in the load transfer mechanism. Five reference points (RP) per floor were defined for possible locations of pushover displacement: one reference node at each location of the connecting angles and one at each West and East panel zones. The story displacements were applied to the reference nodes according to the experimental sequences shown in Fig. 2. Having displacement records for each story available, an independent displacement-control for each story could be

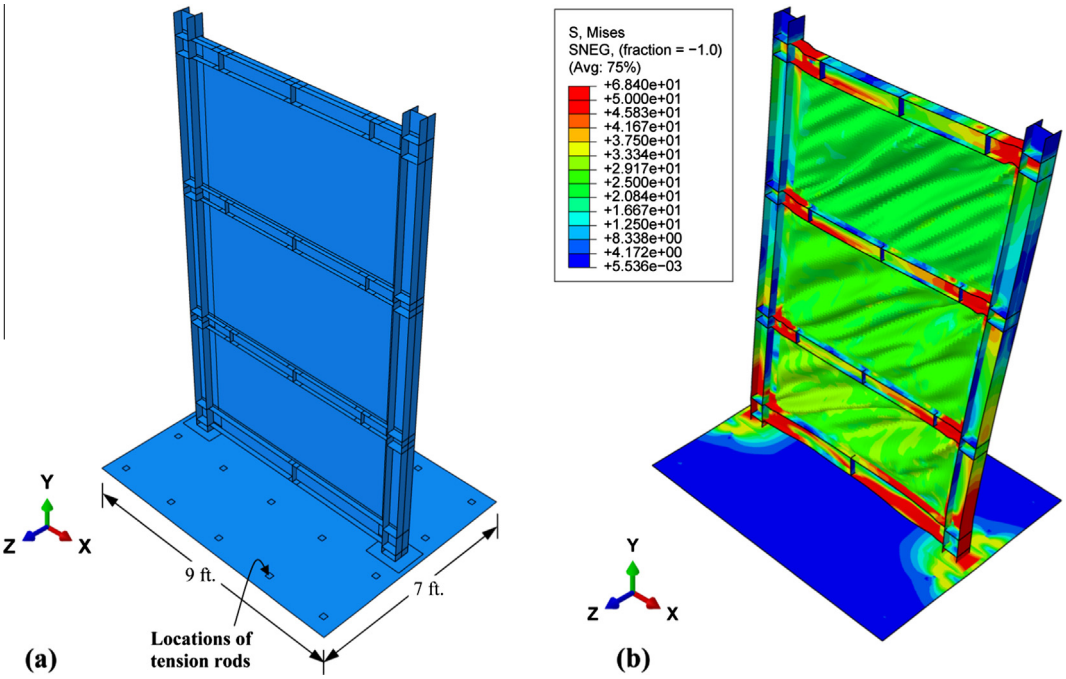

Fig. 11. Finite element analysis: (a) model; (b) stress contours at +3.33% drift.

applied in the FE model to simulate the loading protocol applied in the experiment.

To help initiate panel buckling and development of tension field action, an initial imperfection was applied to the model analyzed. The shape of imperfection was a summation of the first eight eigenmodes of every panel (i.e., total 24 eigenmodes). Based on recommendations of a previous study (i.e., [18]), scale factors equal to 1, ½, and ¼ were selected respectively for the first and second modes, the third to fifth modes, and the sixth to eight modes of each panel. The resulting imperfection magnitudes corresponded to only a few percent of the shell thickness.

The cyclic pushover analysis was conducted following the displacement history presented in Fig 2 with several modifications. Several steps performed during the experiment (i.e., Step 6a, 6b, 7b, 9a, 10a, 10b, 10c) were excluded from the finite element analysis to reduce computational complexities. For the same reason, it

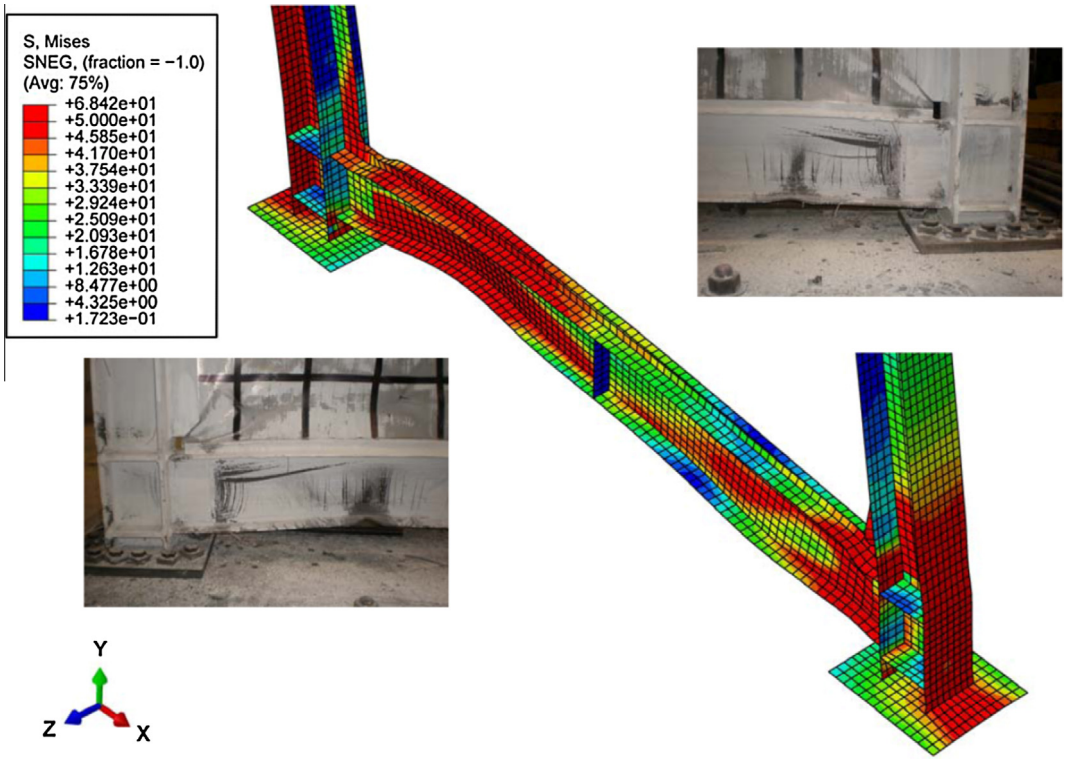

Fig. 12. Analytical deformed shapes with stress contours of HBE0 at −3.33% drift.

was decided to perform only one cycle per analysis step instead of the 2 or 3 cycles conducted during the experiment. Though slight differences in the displacement histories in the positive and negative directions were observed during the experiment, all displacement excursions were taken as symmetric in the finite element analysis and the displacement history in the positive direction was used as the reference for this purpose.

Fig. 7 shows the resulting hysteresis of base shear versus lateral displacement at the top floor. The finite element analysis results capture the experimental strength well in the positive direction while it slightly underestimates that in the negative direction. However, the pinching behavior obtained in the analysis is not as severe as that observed during the experiment. The analytical deformed shape with stress contours shown in Fig. 11b displays the amount of yielding in the FEM model at 3.33% drift. Plastification of the horizontal boundary elements is observed not only at the HBE ends but also along their spans. Fig. 12 presents a close up view of the HBE0 plastification and compares it to the specimen condition at the end of the test. The finite element results resemble the specimen response observed during the experiment.

Vertical deformations of HBE3, HBE2, and HBE0 obtained from the finite element analysis are presented in Fig. 8b compared to those recorded during the experiment. Overall, the finite element results show the accumulation of plastic incremental deformation similar to that was observed during the experiment. However, their magnitudes were significantly smaller compared to those recorded during the experiment. In the last displacement cycle (when the FEM model was cycled up to 3.33% top story drift amplitude), the vertical deformations were 0.56 (upward), 0.36, and 0.39 in. for HBE0, HBE2, and HBE3, respectively. In contrast, the vertical deformations recorded during the experiment for the same respective HBEs were 1.64 (upward), 0.74, and 1.12 in. Consequently, a complete plate yielding in the FEM model occurred quicker in the FEM model compared to that observed in the experiment.

It is suspected that the decision to exclude several displacement steps from the analysis and to conduct only one cycle per displacement step; as well as the fact that the FEM model was not developed to consider material fatigue life, contributed to this discrepancy. It was also observed that the finite element results exhibited more severe local buckling at the ends of the HBE than observed experimentally (Fig. 12). The reasons for this discrepancy are unclear but partly attributable, again, to errors introduced by the detailing used for load transfer to the specimen. Hopefully, future research, benefiting from the knowledge generated during this experimental program, will be able to generate additional experimental data tailored for validation by finite analysis results to further investigate the causes for the above discrepancies.

7. Conclusions

A 1/3-scale model of three-story SPSW specimen was designed and tested to investigate the impact of in-span hinges on the seismic behavior of steel plate shear walls. The experiment demonstrated the development of in-span plastification and accumulation of plastic incremental deformations predicted to develop. These findings suggest that development of in-span hinges should be explicitly avoid in the design of HBEs. This research also allowed to experimentally observe that the moment–rotation hysteresis curves of HBEs connections in SPSWs are not symmetric, but rather lopsided toward one direction, unlike what is typically observed in special moment-resisting frames. Special moment connections were used to connect HBEs to VBEs due to expected larger rotations in SPSWs having in-span hinging. While several of those special moment connections remained intact up to the conclusion of the test, some special moment connections experienced fractures. These connections were found to be those subjected to the higher rotation range prior to fracture (but not largest absolute rotations). While additional experimental investigations would provide further information, this finding suggests that, in some instances, the ordinary-type connection specified by the code (i.e., [1]) to be used in SPSWs might not be sufficient to sustain large rotation demand that could occur in the connections. A finite element investigation of the tested specimen showed similar overall behavior to that observed during the experiment. Future research is needed to assess how various SPSW configurations (e.g., number of stories, different infill plate aspect ratios, different relative stiffness between HBEs, presence of composite slabs) would affect the development of in-span plastic hinge. A full scale testing would be desirable to validate findings of this research and to investigate different lateral load profiles and different loading protocols (e.g. shake table and pseudo-dynamic tests).

Acknowledgments

This work was supported in part by the George E. Brown, Jr. Network for Earthquake Engineering Simulation (NEES) Program of the National Science Foundation under NSF NEESR Award Number CMMI-0830294. W-steels used for this study were donated by the American Institute of Steel Construction (AISC). Niagara Testing performed nondestructive inspection on several special moment connections. The financial support of the Universitas of Bandar Lampung, Indonesia to the first author is gratefully appreciated. However, any opinions, findings, conclusions, and recommendations presented in this paper are those of the writers and do not necessarily reflect the views of the sponsors.

References

[1] AISC. Seismic provisions for structural steel buildings. ANSI/AISC 341-10. American Institute of Steel Construction, Inc., Chicago, Illinois; 2010.
[2] AISC. Prequalified connections for special and intermediate steel moment frames for seismic applications. ANSI/AISC 358-10. American Institute of Steel Construction, Inc., Chicago, Illinois; 2010.
[3] ASCE. Minimum design loads for buildings and other structures. ASCE/SEI 7-10. American Society of Civil Engineers, Reston, Virginia; 2013.
[4] ATC-24. Guidelines for cyclic seismic testing of components of steel structures. Applied Technology Council, Redwood City, CA; 1992.
[5] Berman JW, Bruneau M. Experimental investigation of light-gauge steel plate shear walls. J Struct Eng ASCE 2005;131(2):259–67.
[6] Berman JW. Seismic behavior of code designed steel plate shear walls. Eng Struct 2011;33(1):230–44.
[7] Bruneau M, Uang CM, Sabelli R. Ductile design of steel structures. 2nd ed. New York: McGraw-Hill; 2011.
[8] Canadian Standards Association (CSA). Design of steel structures. CAN/CSA S16-09. Willowdale, Ontario, Canada; 2009.
[9] Choi I-R, Park H-G. Steel plate shear walls with various infill plate designs. J Struct Eng ASCE 2009;135(7):785–96.
[10] Dassault Systèmes. ABAQUS/standard user's manual. Version 6.9-1. Dassault Systèmes Simulia Corporation, Providence, Rhode Island; 2009.
[11] Dastfan M. Ductile steel plate shear walls with PEC columns. PhD dissertation. University of Alberta, Edmonton, Alberta, Canada; 2011.
[12] Dowden D, Bruneau M. Analytical and experimental investigation of resilient self-centering steel plate shear walls. Tech. rep. MCEER-14-0010. Multidisciplinary Center for Earthquake Engineering Research, State University of New York at Buffalo, Buffalo, New York; 2014.
[13] Driver RG, Kulak GL, Kennedy DJL, Elwi AE. Seismic behavior of steel plate shear walls. Structural engineering report 215. Department of Civil Engineering, University of Alberta, Edmonton, Alberta, Canada; 1997.
[14] FEMA. State of the art report on systems performance of steel moment frames subject to earthquake ground shaking. FEMA report no. 355C. Prepared by the SAC Joint Venture Partnership for the Federal Emergency Management Agency, Washington, DC; 2000.
[15] FEMA. NEHRP recommended provisions for seismic regulations for new buildings and other structures. FEMA report no. 450. Building Seismic Safety Council for FEMA, Washington, DC; 2003.
[16] Hitaka T, Matsui C. Experimental study on steel shear wall with slits. J Struct Eng ASCE 2003;129(5):586–95.

[17] Kusumastuti D, Reinhorn AM, Rutenberg A. A versatile experimentation model for study of structures near collapse applied to seismic evaluation of irregular structures. Technical rep. no. MCEER-05-0002. Multidisciplinary Center for Earthquake Engineering Research, Buffalo, New York; 2005.
[18] Purba R, Bruneau M. Finite element investigation and design recommendations for perforated steel plate shear walls. J Struct Eng ASCE 2009;135(11):1367–76.
[19] Purba R, Bruneau M. Case study on the impact of horizontal boundary elements design on seismic behavior of steel plate shear walls. J Struct Eng ASCE 2012;138(5):645–57.
[20] Purba R, Bruneau M. Seismic performance of steel plate shear walls considering various design approaches. Tech. rep. MCEER-14-0005. Multidisciplinary Center for Earthquake Engineering Research, State University of New York at Buffalo, Buffalo, New York; 2014.
[21] Qu B, Bruneau M, Lin CH, Tsai KC. Testing of full scale two-story steel plate shear walls, with RBS connections and composite floor. J Struct Eng ASCE 2008;134(3):364–73.
[22] Rezai M. Seismic behavior of steel plate shear walls by shake table testing. PhD dissertation. University of British Columbia, Vancouver, BC, Canada; 1999.
[23] Roberts T, Sabouri-Ghomi S. Hysteretic characteristics of unstiffened plate shear panels. Thin Wall Struct 1991;12(2):145–62.
[24] Sabelli R, Bruneau M. Steel plate shear walls (AISC design guide). Chicago, Illinois: American Institute of Steel Construction, Inc.; 2007. 144 p.
[25] Vian D, Bruneau M. Steel plate shear walls for seismic design and retrofit of building structures. Tech. rep. MCEER-05-0010. Multidisciplinary Center for Earthquake Engineering Research, State University of New York at Buffalo, Buffalo, New York; 2005.